J Solid State Electrochem (2010) 14:515–521
DOI 10.1007/s10008-008-0727-8

ORIGINAL PAPER

Analysis of the influence of rhodium addition to platinum on its activity towards methanol electrooxidation by EIS

Wojciech Tokarz · Piotr Piela · Andrzej Czerwiński

Received: 30 June 2008 / Revised: 21 October 2008 / Accepted: 3 November 2008 / Published online: 27 November 2008

Abstract Influence of rhodium addition to platinum on the activity of the alloy in methanol electrooxidation has been studied using Pt–Rh/Au limited volume electrodes with various surface compositions including the pure Pt and Rh metals. Electrochemical impedance spectroscopy (EIS) was used in the study. In the case of the Pt–Rh alloy, the impedance picture of methanol oxidation is qualitatively the same as for the pure Pt electrode. However, impedance spectra strongly depend on alloy composition. Equivalent circuits suitable for methanol oxidation on Pt were also used in the case of Pt–Rh and similar fitting results were obtained. A reaction mechanism suggested in the literature for Pt, which involves two strongly adsorbed intermediates competing for the same adsorption sites, is likely also for the Pt–Rh alloys. However, fittings with a corresponding impedance model were unsuccessful for both Pt and Pt–Rh because of mathematical caveats, such that quantitative comparisons were not possible. Nevertheless, EIS results suggest that Rh inhibits the kinetics of formation of reactive oxygen species at the surface of the alloy.

Keywords Methanol · Electrooxidation · Pt–Rh alloy · Electrochemical impedance spectroscopy · EIS

Contribution to the Fifth Baltic Conference on Electrochemistry, 30 April - 3 May 2008, Tartu, Estonia.

W. Tokarz · P. Piela · A. Czerwiński (✉)
Industrial Chemistry Research Institute,
Rydygiera 8,
01-793 Warsaw, Poland
e-mail: andrzej.czerwinski@ichp.pl
e-mail: aczerw@chem.uw.edu.pl

W. Tokarz · A. Czerwiński
Faculty of Chemistry, Warsaw University,
Pasteura 1,
02-093 Warsaw, Poland

Introduction

Electrooxidation of methanol has been widely studied on various electrodes [1–4] in order to improve direct methanol fuel cell efficiency. A mechanism of this reaction on platinum is accepted [5], in which, in a series of initial steps, methanol adsorbs on Pt atoms and dehydrogenates forming strongly adsorbed CO:

$$CH_3OH + Pt \rightarrow Pt - CH_2OH + H^+ + e \quad (1)$$

$$Pt - CH_2OH + Pt \rightarrow Pt_2 - CHOH + H^+ + e \quad (2)$$

$$Pt_2 - CHOH + Pt \rightarrow Pt_3 - COH + H^+ + e \quad (3)$$

$$Pt_3 - COH \rightarrow Pt - CO + 2Pt + H^+ + e \quad (4)$$

In the following, adsorbed CO reacts with active surface oxide species simultaneously generated from water with release of CO_2:

$$Pt + H_2O \rightarrow Pt - OH + H^+ + e \quad (5)$$

$$Pt - CO + Pt - OH \rightarrow CO_2^{(\uparrow)} + 2Pt + H^+ + e \quad (6)$$

Reaction 5 requires the highest electrode potential to occur and is the rate-determining step (RDS) at lower values of electrode potential. To accelerate the RDS, a fraction of Pt can be replaced by other elements, for which reaction 5 is facilitated. The whole process occurs then according to the bifunctional mechanism [6], in which the role of Pt is to reactively adsorb methanol and the role of the second metal is to reactively adsorb water. To date,

Pt–Ru alloys have exhibited the best catalytic activity towards methanol electrooxidation. Ruthenium has much greater ability, compared to Pt, to form surface oxide species and also it has a lower d-band electron density than Pt. The latter feature makes Ru capable of weakening the bond between the strongly adsorbed CO and Pt by withdrawing electron density from the bond—the ligand effect [7].

In cyclic voltammetry, rhodium shows a significant negative shift in the onset potential of surface oxide formation, relative to Pt, which is approximately 300 mV [8]. This indicates that Rh used as the second metal in a Pt-based alloy could provide for a bifunctional effect similar to ruthenium. The influence of Rh as second metal in the Pt-based alloy on methanol electrooxidation has been described in our previous papers [8, 9], in which we presented the results of stripping and continuous methanol electrooxidation. Conclusion from this work is that there exists a relationship between Pt–Rh alloy surface composition and methanol adsorption product oxidation potential. The biggest shift in oxidation potential, relative to Pt, exhibited an alloy with about 65 at.% of Rh and the potential shift was only about 50 mV towards cathodic potentials. Also, it was observed that the Rh component in the Pt–Rh alloy inhibits the activity of the Pt component in continuous methanol oxidation, such that 15 times lower current density is observed on the Pt component in the Pt–Rh alloy compared with pure Pt. The proposed mechanistic causes of the poor catalytic performance of the Pt–Rh alloy included [8]: (1) slow dehydrogenative methanol adsorption (reactions 1–4), (2) slow reactive water adsorption (reaction 5), and (3) slow combination of methanol adsorption products with surface oxygen species (reaction 6). The first possibility was excluded by measuring the kinetics of methanol adsorption on pure metals and on Pt–Rh alloy electrodes. It was found that the Pt component of the alloy accelerates the kinetics of methanol adsorption for Pt–Rh to the level observed for pure Pt.

Using electrochemical impedance spectroscopy (EIS), researchers have studied the electrooxidation of H_2/CO on Pt [10, 11] and methanol on Pt [12–15] and Pt–Ru [16–20] alloys. EIS applied to these processes, which involve strongly adsorbed intermediates, has been shown to be capable of distinguishing the details of the reaction mechanism. In the present study, we applied the technique to compare the electrooxidation of methanol on Pt and Pt–Rh electrodes and to understand why there is no benefit from introducing Rh to Pt in methanol electrooxidation.

Experimental

All working electrodes used in this study were limited volume electrodes (LVEs) [21–23], which were electrodeposited potentiostatically on 0.5-mm-diameter gold wires (99.99 Au) from aqueous solutions containing H_2PtCl_6, $RhCl_3$, and HCl. The procedure for obtaining a Pt–Rh electrode surface with a precisely defined surface composition is described in detail in [8]. The deposited layer thickness was a few micrometers and the surface roughness factor was in the range 50–200. The working electrode wire was placed in a small glass cell together with a large gold sheet serving as the counter electrode and a saturated KCl calomel reference electrode. The reference electrode was isolated from the working electrode compartment with the use of an electrolytic key closed with a piece of Nafion® 117 membrane and filled with the working electrolyte solution. The relative positioning of the electrodes in the cell was kept the same from experiment to experiment. All potentials given in this work are versus the standard hydrogen electrode (SHE) and were obtained by adding the table value of 0.244 V to the measured potential.

All electrochemical studies were performed in deoxygenated ultrapure (Millipore, 18 MΩ cm) aqueous 0.5 M H_2SO_4 solutions at room temperature. Methanol concentration of 1 M was used. All chemicals used were of high-purity grade and were used without additional purification. Prior to impedance experiments, the electrodes were cleaned by in situ electrochemical cycling in the potential range 0.050–1.250 V at 0.050 V s^{-1} to obtain well-defined voltammograms certifying high system purity. For 20 min before impedance recording, the cell was equilibrated at the chosen direct current (DC) potential level and this steady-state DC potential value was used as the DC level during the quasi-potentiostatic EIS experiment. The impedance spectra were recorded at ten points per decade of frequency with 10-mV true amplitude (peak-to-peak/2) and in the frequency range from 100 kHz to 5 mHz. In cases when obtained impedance spectra showed a significant influence of noise at low frequencies, only noise-free parts of the spectra were taken for fitting and are presented on graphs. Spectra corresponding to a narrowed frequency range are marked by the lowest frequency value placed near the corresponding data point. All electrochemical techniques were performed with a Volta-Lab PGZ 301 potentiostat–galvanostat. EIS spectra were fitted to equivalent circuits using ZView software (Scribner Associates, USA) incorporating a complex nonlinear least squares fitting algorithm.

Results and discussion

All prepared LVE deposits had the typical form of metal black characterized by good adhesion and completely homogenous alloy composition. Figure 1 shows scanning electron microscopy (SEM) images of Pt/Au LVE and Pt–Rh/Au LVE with 60% of Rh on the surface. No significant difference in morphologies of these surfaces is

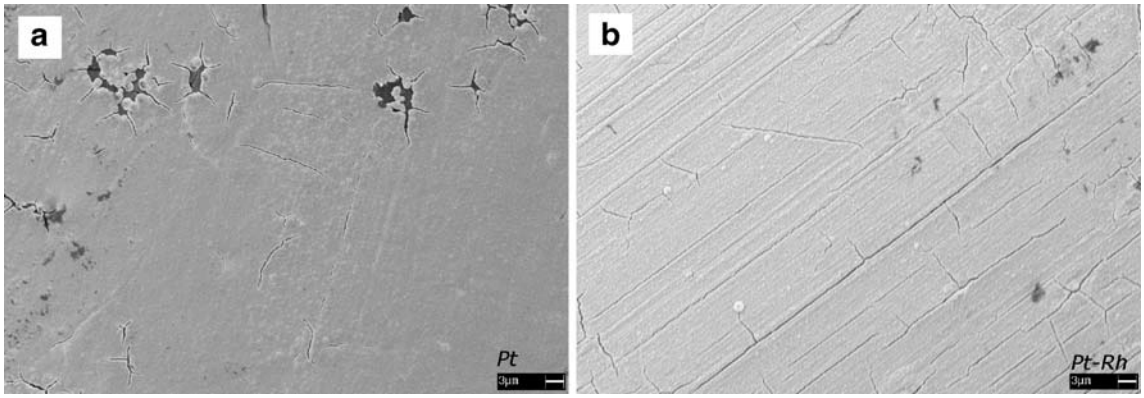

Fig. 1 SEM image of **a** Pt/Au LVE and **b** Pt–Rh/Au LVE (60% Rh)

noticeable. Both electrodes are characterized by a similar roughness factor. Therefore, we can compare the activity of both electrodes without the risk of influence of morphology on the results of methanol electrooxidation investigation.

Impedance spectra of methanol electrooxidation recorded on the Pt/Au LVE electrode are consistent with impedance spectra of the same process occurring on smooth polycrystalline Pt [12] as well as on Pt nanoparticles supported on a high-surface-area carbon [13]. At low steady-state electrode potentials, the Nyquist plots have the form of a large arc in the first quadrant of the −imaginary (−*Z*') vs. real (*Z*') impedance part plane (Fig. 2a). Upon increasing the electrode potential, Nyquist plots decrease in diameter and at low frequencies the spectra enter the fourth quadrant. The large arcs reflect slow methanol adsorption kinetics at low electrode potentials, at which strongly adsorbed CO—the reaction intermediate—blocks the electrode surface. Increasing potential is a driving force for the reaction, so the impedance of charge transfer becomes smaller, and, consequently, recorded Nyquist plots are smaller, too. When electrode potential exceeds 0.520 V, a pseudo-inductive impedance arc forms at low frequencies in the fourth quadrant of the −*Z*' vs. *Z*' plane. Further increasing electrode potential causes growing of the pseudo-inductive arc (Fig. 2b). This pseudo-inductive behavior of impedance is characteristic for processes involving a strongly adsorbed intermediate [24]. When the surface coverage by the strong adsorbate—CO in this case—responds slowly to the alternating electrode potential, there is a delay between the potential perturbation and the resulting alternating current being a function of the coverage. This results in a pseudo-inductance. Shifting electrode potential even higher, above 0.620 V, brings another change to the impedance behavior. Arcs in the first and fourth quadrants start to grow rapidly with potential and, when the potential reaches 0.665 V, the Nyquist plot flips from the first and fourth quadrants to the second and third quadrants (Fig. 2c). On the Bode plot of the impedance phase angle (theta) vs. perturbation frequency (Fig. 2d), this characteristic flip of the −*Z*' vs. *Z*' plane spectra appears as a discontinuity of the plot. The flip occurs at potentials, at which adsorption products start to oxidize, and on the stripping curve we observe the growth of an adsorbate oxidation peak (not shown, see [8]).

Such an evolution of impedance spectra with potential is characteristic for a situation, when there are two adsorbate species competing for the same adsorption sites and there is a potential-induced change of the RDS [25]. In the case of methanol electrooxidation on Pt, the two adsorbing species are CO from methanol adsorption and OH from water adsorption. At low potentials, the RDS is OH formation. As the electrode potential is increased, OH formation accelerates and, at a sufficiently high potential, it becomes faster than the reaction between surface CO and surface OH. This latter process becomes the new RDS [13].

The impedance picture of methanol oxidation on Pt–Rh alloys is qualitatively the same as for pure Pt. At low steady-state electrode potentials, the capacitive impedance arcs have large diameters indicating the strong blocking effect of CO adsorption on methanol oxidation. Those impedance arcs become smaller as the electrode potential increases and pseudo-inductive arcs appear in the fourth quadrant (Fig. 3a). Further increase of electrode potential brings an increase of arcs' diameters and a subsequent flip of the −*Z*' vs. *Z*' plot to the second and third quadrants. Notably, the transition of the spectrum from the first and fourth to the second and third quadrants occurs at much higher electrode potentials and spans over a wider potential range than it was the case on Pt. Having in mind the mechanistic causes of these transformations, one can conclude that: (1) the CO and OH adsorbates compete for the same adsorption sites on the alloy's surface, which is a confirmation of the fact that methanol adsorbs on Pt as well as on Rh and, (2) for the Pt–Rh electrode, either the increase of the rate of active oxygen species formation with electrode potential is much slower than for Pt or the increase of the rate of reaction between methanol adsorption products and surface OH with electrode potential is

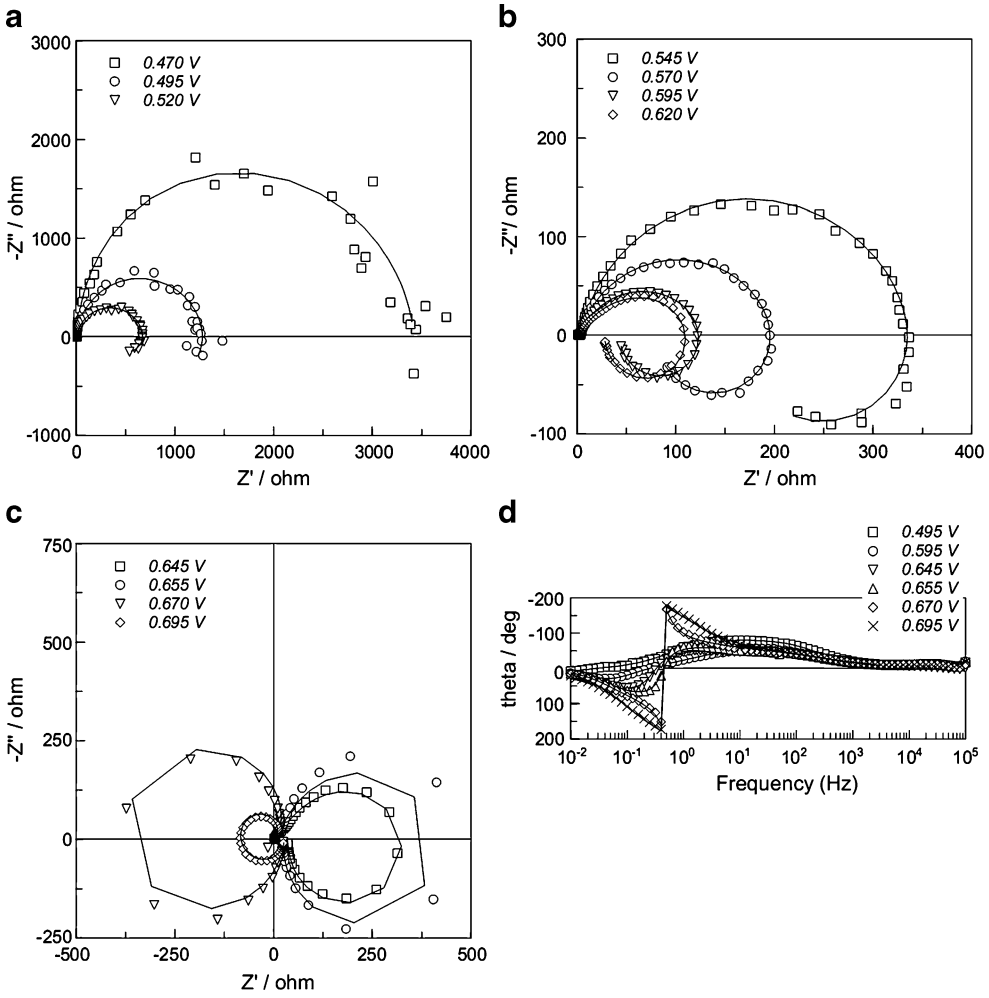

Fig. 2 Experimental (*points*) and fitted (*lines*) EIS plots of methanol electrooxidation on Pt/Au LVE at different steady-state electrode potentials. **a**–**c** Nyquist and **d** Bode phase-angle plots, 1 M CH_3OH, 0.5 M H_2SO_4, frequency range 100 kHz to 5 mHz, room temperature. Fitted plots were obtained using model circuits of Fig. 5a (see text for details)

much faster than for Pt or both. The latter effect caused by a less energetically stable adsorption layer on Pt–Rh, relative to Pt, is a fact; however, it is less probable to influence the evolution of impedance spectra because the difference in stripping potentials on Pt–Rh and Pt is relatively small (less than 0.05 V).

The alloy's surface composition has a strong influence on the spectra (Fig. 4). Most notably, as the Rh content decreases, the charge transfer kinetics of the process becomes faster. It indicates that the platinum component of the alloy plays the most important role in methanol electrooxidation activity of the Pt–Rh system. Moreover, at the high steady-state electrode potential used for recording Fig. 4 data, which is higher than the potential of the spectrum flip to the second and third quadrants observed for Pt, decreasing the Rh content as low as 11% does not cause the flip. To observe the flip upon Rh removal, a potential of 0.845 V was needed (Fig. 3b,c). This indicates that even a small amount of Rh added to Pt strongly influences the catalytic properties of Pt in methanol oxidation by inhibiting the kinetics of surface oxide formation.

All solid-line curves shown on impedance plots come from fitting of model equivalent circuits to the experimental data. Two equivalent circuits have been proposed in the literature to describe methanol oxidation on Pt. The first one was based on a reaction mechanism involving only one adsorbed intermediate (Fig. 5a, top circuit). It was developed by Harrington and Conway [24] and, in an alternative but equivalent form, first used for methanol electrooxidation by Melnick and Palmore [12]. The second was derived from a reaction model involving two adsorbed intermediates. It was proposed by Cao [25] and adopted to methanol electrooxidation by Hsing et al. [13] (Fig. 5b). Both equivalent circuits have been used to fit the experimental data shown in this paper in order to compare their applicability. The results of this exercise can be summarized as follows.

The full model circuit of Fig. 5a (top circuit) gave good fitting results characterized by low standard deviations of the whole fit [26, 27] for all data shown in Fig. 2, except for two cases: at lowest steady-state electrode potentials (0.470 and 0.495 V in Fig. 2a) and at a steady-state potential

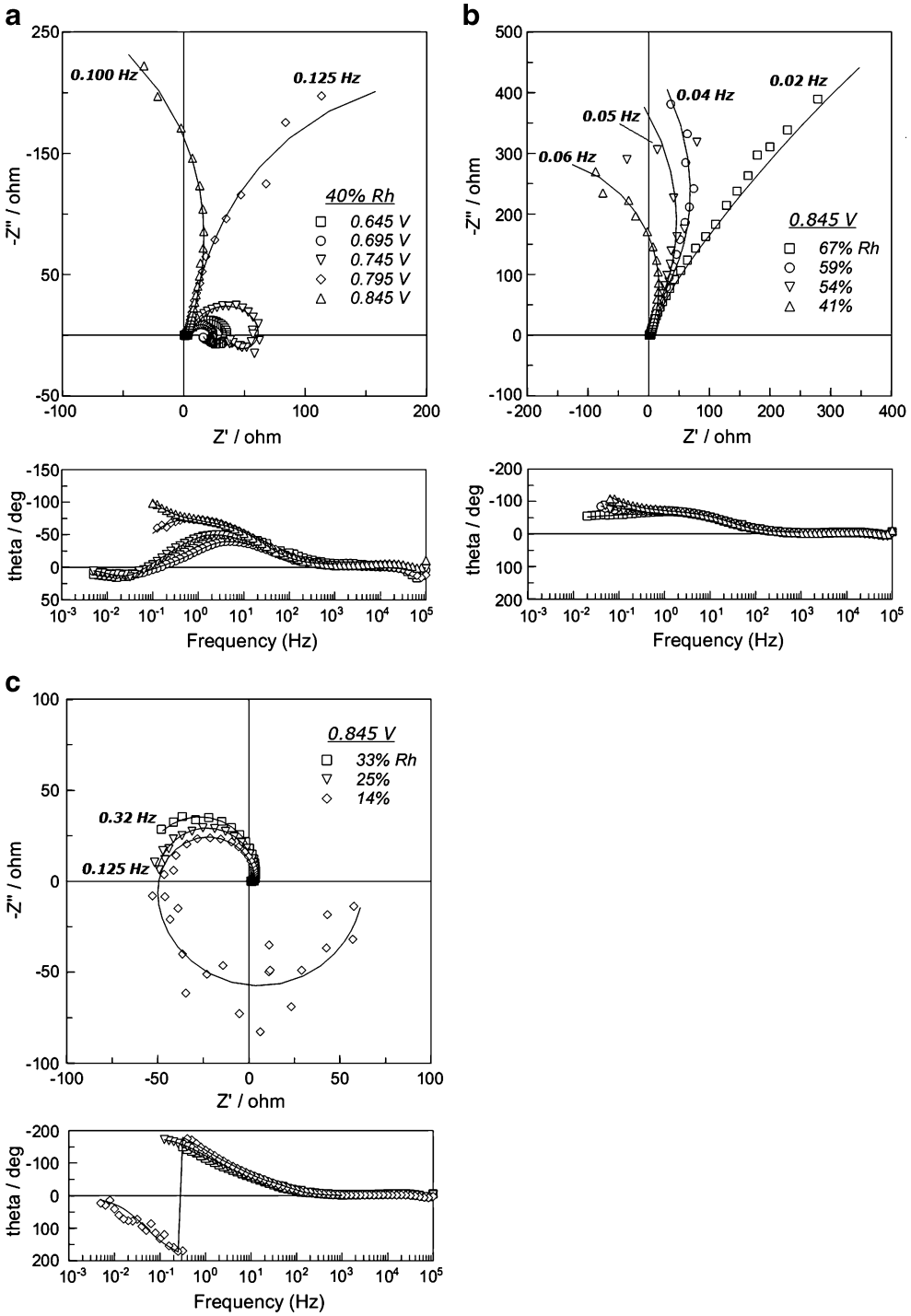

Fig. 3 Experimental (*points*) and fitted (*lines*) Nyquist (*upper graphs*) and Bode phase-angle (*lower graphs*) plots of methanol electrooxidation on Pt–Rh/Au LVEs at: **a** different steady-state electrode potentials and fixed alloy composition (40% Rh), and **b**, **c** fixed steady-state electrode potential (0.845 V) and different alloy compositions. Experimental conditions: 1 M CH_3OH, 0.5 M H_2SO_4, frequency range 100 kHz to 5 mHz (for narrowed frequency range due to noise at low frequencies, the lowest frequency is marked on plot), room temperature. Fitted plots were obtained using model circuits of Fig. 5a (see text for details)

closest to the flip of the spectrum to the second and third quadrants (0.655 V in Fig. 2c). In the first case, the R3 and the L elements of Fig. 5a became redundant (high best-fit estimates and high errors of best-fit estimates), so the equivalent circuit was reduced to the one in Fig. 5a, middle, which is more consistent with the actual spectral features present in those data. In the more interesting second case, the charge transfer resistance (R2 in Fig. 5a) became redundant (very high best-fit estimate and its error equal 100%), and the equivalent circuit was reduced to the bottom one in Fig. 5a. Since there is no mechanistic reason for the charge transfer resistance to become very large at the potential of the spectrum flip (see below), this might indicate that the one-adsorbate model may be inadequate for the studied process. Nevertheless, after these reductions, good fitting quality was obtained also for these standing-out datasets. These results are consistent with the results of Seland et al. [15].

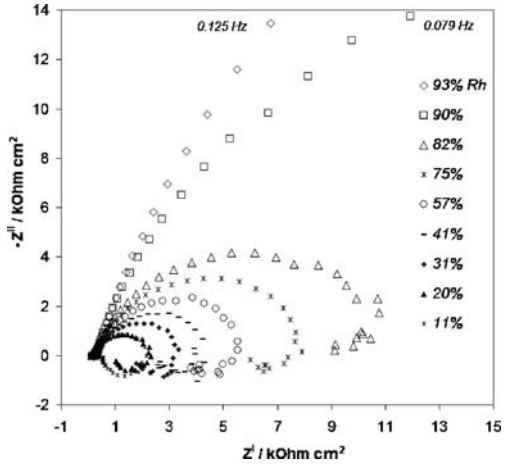

Fig. 4 Experimental Nyquist plots of methanol electrooxidation on Pt–Rh/Au LVEs of various surface compositions at 0.745 V steady-state electrode potential. 1 M CH_3OH, 0.5 M H_2SO_4, frequency range 100 kHz to 5 mHz, room temperature

The model based on one adsorbed intermediate could only describe the change in RDS (flip of Nyquist plot to the second and third quadrants) if negative values of charge transfer resistance (R2 in Fig. 5a) were allowed. The charge transfer resistance equal to the steady-state derivative $\partial\eta/\partial i$, i.e., the reciprocal of the slope of a steady-state polarization plot (η—overpotential; i—current density), can be negative for processes involving potential-dependent blocking effects. For such processes, there are regions of the steady-state i–η curve, in which the steady-state current density falls with increasing overpotential. In the case of methanol electrooxidation on Pt, such a blocking effect indeed occurs and is related to passivation of the electrode surface by a dense oxide layer preventing methanol adsorption. However, the passivation and the resulting negative charge transfer resistance occur in a potential region above 0.8 V vs. SHE [8, 13, 20]. At these potentials, the impedance spectrum is already flipped to the second and third quadrants of the $-Z$'' vs. Z' plane. As seen in our data (Fig. 2c), which is in very good agreement with literature data on this process [12, 13], the flip occurs at 0.665 V vs. SHE. Since between 0.665 V and (at least) 0.800 V vs. SHE the charge transfer resistance is positive, the simpler equivalent circuit cannot be used to fit the flipped spectra as it requires negative values of the charge transfer resistance to give an acceptable fit.

The more complicated equivalent circuit of Fig. 5b is fundamentally more adequate. As shown by Hsing et al. [13], with one set of kinetic parameters, it allows correct simulation of the evolution of impedance spectra with steady-state electrode potential for the reaction of methanol on Pt. Also, flipped spectra can be simulated using positive values of the charge transfer resistance (R2 in Fig. 5b), so there is agreement with polarization experiments. However, when this model circuit was used to fit the Fig. 2 data, poor fits were obtained in all cases as judged by high values of the standard deviations of the whole fit. Moreover, looking at the errors of the best-fit parameter estimates, it was impossible to consistently remove redundant elements from the circuit because the fitting procedure converged quite randomly to different local minima of the sum of squares. This happened despite applying common techniques for finding the global minimum in nonlinear least squares fitting [26]. Interestingly, it was impossible to detect the poor fitting quality only by looking at the Nyquist and the Bode plots. In fact, the fits obtained with the Fig. 5a circuit, which were characterized by low standard deviations,

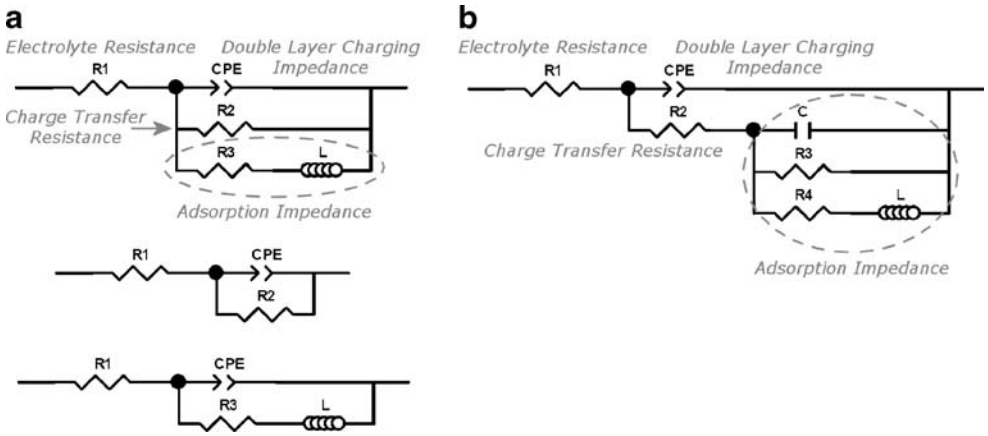

Fig. 5 Equivalent circuits suitable for describing methanol electrooxidation. **a** Single adsorbed intermediate and **b** two adsorbed intermediates competing for the same adsorption sites. Two simpler circuits in **a** are reduced versions of the top circuit, which are suitable for fitting experimental EIS data obtained at certain values of the steady-state electrode potential (see text for details). Meaning of circuit elements is indicated on the graphs. Double-layer charging was modeled as a constant phase element (*CPE*). Elements constituting the adsorption impedances are complicated functions of various steady-state derivatives of electrode coverage by adsorbed intermediates over time and electrode potential [24, 25]

almost overlapped with those obtained using the Fig. 5b circuit yielding much higher standard deviations. Apparently, fitting with the circuit of Fig. 5b constituted an example of a poor fitting situation. It was most likely caused by the combined effect of a complicated character of the impedance spectra (points in all four quadrants of the $-Z$' vs. Z' plane), a large data scatter at low frequencies, and a high nonlinearity of the model Z function for the circuit of Fig. 5b [27].

The presented fitting situation repeated itself in the case of methanol electrooxidation on the Pt–Rh electrodes (Fig. 3). To summarize, failure to fit the impedance spectra for methanol electrooxidation on the Pt/Au LVE and the Pt–Rh/Au LVEs with the fundamentally adequate but complicated model circuit of Fig. 5b limited the present interpretation of EIS results to qualitative conclusions. Even with the present, relatively noisy, dataset, it is perhaps possible to obtain good fits of the Fig. 5b model by using the admittance instead of the impedance function or by using other mathematical transformations of the model in order to decrease nonlinearity [27]. This will be part of future efforts.

Conclusions

Electrochemical impedance analysis of the influence of rhodium addition to platinum on the activity towards methanol electrooxidation suggests that even small amounts of rhodium slow down the kinetics of oxide layer formation on the alloy electrode. It contributes to the understanding of previous observations that rhodium accompanying platinum in the alloy strongly inhibits the activity of the platinum surface in continuous methanol electrooxidation.

Acknowledgements Statutory funding from the Industrial Chemistry Research Institute, Warsaw, and the Department of Chemistry, Warsaw University, is greatly acknowledged.

References

1. Iwasita T (2002) Electrochim Acta 47:3663, and errata 48:289 2
2. Bogotzky VS, Osetrova NV, Skundin AM (2003) Electrokhim 39:919
3. Liu H, Song C, Lei Z, Zang J, Wang H, Wilkinson DP (2006) J Power Sources 155:95
4. Antolini E (2007) Appl Catal B 74:337
5. Aricó AS, Srinivasan S, Antonucci V (2001) Fuel Cells 1:133
6. Watanabe M, Motoo S (1975) J Electroanal Chem 60:275
7. Tong Y, Kim HS, Babu PK, Waszczuk P, Wieckowski A, Oldfield E (2002) J Am Chem Soc 124:468
8. Tokarz W, Siwek H, Piela P, Czerwiński A (2007) Electrochim Acta 52:5565
9. Siwek H, Tokarz W, Piela P, Czerwiński A (2007) J Power Sources 181:24
10. Leng Y-J, Wang X, Hsing I-M (2002) J Electroanal Chem 528:145
11. Wang X, Hsing I-M, Leng Y-J, Yue P-L (2001) Electrochim Acta 46:4397
12. Melnick RE, Palmore GTR (2001) J Phys Chem B 105:1012
13. Hsing I-M, Wang X, Leng Y-J (2002) J Electrochem Soc 149: A615
14. Otomo J, Xiaoen L, Takeshi K, Ching-ju W, Hidetoshi N, Hiroshi T (2004) J Electroanal Chem 573:99
15. Seland F, Reidar T, Harrington DA (2006) Electrochim Acta 51:3827
16. Müller JT, Urban PM, Hölderich WF (1999) J Power Sources 84:157
17. Gang W, Li L, Xu B-Q (2004) Electrochim Acta 50:1
18. Chakraborty D, Chorkendorff I, Johannessen T (2006) J Power Sources 162:1010
19. Piela P, Fields R, Zelenay P (2006) J Electrochem Soc 153:A1902
20. Wang Z-B, Yin G-P, Shao Y-Y, Yang B-Q, Shi P-F, Feng P-X (2007) J Power Sources 165:9
21. Czerwiński A, Marassi R, Sobkowski J (1984) Ann Chim Rome 74:681
22. Czerwiński A, Zamponi S, Marassi R (1991) J Electroanal Chem 304:233
23. Czerwiński A, Marassi R, Zamponi S (1991) J Electroanal Chem 316:211
24. Harrington DA, Conway BE (1987) Electrochim Acta 32:1703
25. Cao CH-N (1990) Electrochim Acta 35:837
26. Macdonald JR (2007) LEVM/LEVMW manual v. 8.08. http://www.solartronanalytical.com, February
27. Zoltowski P (2005) Solid State Ionics 176:1979